Chapter 2

Experiments

This chapter will present the process of manufacturing high quality ($Q>10^4$) microstrip ring and line resonators made of YBCO and Ca-YBCO thin films deposited on both sides of $LaAlO_3$ (LAO) substrates by using pulsed laser deposition. The characteristics of superconducting YBCO and Ca-YBCO thin films deposited on LAO (100) substrates were carefully studied by use of X-ray diffraction, atomic force microscopy and resistivity measurements. The films were then patterned into the ring or line pattern by using photolithography and wet etching method. The microwave properties were measured with various hole concentrations by controlling oxygen contents in the same microstrip resonator. The microwave measurement system in our laboratory and the measurement calibrations were also described detailed here.

2.1 Preparation and Characterization of Thin Films

Pulsed laser deposition (PLD) system was used in our experiments to prepare YBCO and Ca-YBCO films deposited on both sides of a 0.5 mm thick $LaAlO_3$ (LAO) substrate. The as-deposited thin films were analyzed by resistivity measurements, X-ray diffraction (XRD) and atomic force microscopy (AFM). The XRD pattern illustrates the epitaxy of YBCO films with (00ℓ) orientation, which is consistent with most results involving the LAO substrate. The surface morphology was characterized by AFM images. In order to fabricate the high-Q microwave device, the surface roughness, grain size and film thickness etc., all of these must be under the well

control condition with epitaxial thin films. This, however, has inevitably complicated both in the fabrication and measurement processes.

2.1.1 Pulsed Laser Deposition System

There have been a variety of in-situ deposition techniques such as sputtering [104], chemical vapor deposition, and pulsed laser deposition (PLD) [105], etc., for preparing highly oriented HTSC films. As is well known, the microstructure of the thin films can affect physical properties [106]. These thin films, although highly oriented and exhibiting superior superconducting properties, are not single crystal. Rather they exhibit a rich microstructure of grain boundaries, stacking faults, dislocations, and other crystallographic defects and interfaces, the characteristics of which depend on the orientation and composition of the films, as well as on the processing parameters. Among many methods the samples we used were prepared by PLD. The PLD method was a ripe technique for the deposition of superhard coating thin films with the stoichiometry of multicomponent compounds. The PLD system, as shown in Fig. 2.1, consists of a laser, an eight-way cross vacuum chamber, vacuum pumps system, a multiple target holder and some other relevant instrumentations.

The same high quality YBCO and Ca-YBCO epitaxial thin films were successfully deposited on both sides of a 0.5 mm thick $LaAlO_3$ (LAO) (100) substrate by PLD method using the KrF excimer laser with the wavelength of 248 nm, the pulsed width of 30 ns, the laser energy of 350 mJ, and a pulse repetition rate of 5 Hz. The chamber was first evacuated to a pressure of about 10^{-6} Torr using a turbomolecular pump prior. The substrate temperature then was kept at 790 ^{0}C for YBCO film and at 760 ^{0}C for Ca-YBCO film with the same oxygen partial pressure of 0.3 torr during the deposition. The substrate temperature was detected

simultaneously during the deposition process by MINOTA Spot Thermometer IR-308. The target was hold parallel to the substrate with a separation of about 4 cm and was rotated during the laser irradiation. The as-deposited films were all c-axis oriented with a typical thickness of 500 nm. The main difficulty for double side deposition was the contact problem between the substrate and the heater. It can be overcome by carefully inserting a thin Si-wafer between the substrate and the heater. This treatment effectively prevents the backside of the polished substrates as well as the first film from contamination during each deposition run.

2.1.2 Structure Characterization of Thin Film

After growing the Ca-YBCO and YBCO thin films, the most important thing is to characterize their physical properties. In this study, we utilized the x-ray diffraction (XRD) to analyze the crystal structure of films and the atomic force microscope (AFM) to observe the surface morphology, and the standard four probe techniques to measure the resistance (resistivity) of the thin films. But, the first important thing for us is to confirm that the substitution of calcium to yttrium in $YBa_2Cu_3O_{7-\delta}$ thin film do not introduce any significant distortion in the YBCO lattice. Tokura *et al.* [35] have found that it was accessible for calcium substituting yttrium in YBCO in the mechanism. Merz *et al.* [36] have used polarization-dependent O 1*s* and Cu 2*p* near-edge x-ray absorption spectroscopy on detwinned $Y_{1-x}Ca_xBa_2Cu_3O_{7-\delta}$ single crystals, where the Ca contents in YBCO single crystal can be up to 30 % . They found that almost Ca^{2+} ions substitutes for Y^{3+} ions, and the substitution of Ca^{2+} ions to Ba^{2+} ions was less than 2 % . Our experimental result (see in Fig. 2.2) shows that most of the Ca^{2+} ions substitutes for Y^{3+} ions from the Ca *L* edge absorption spectra of $Y_{0.7}Ca_{0.3}Ba_2Cu_3O_{6.6}$ thin film by measuring the X-ray absorption near edge structure

(XANES) [107]. The two highest absorption peaks are due to the substitution of calcium to yttrium. The lower absorption peaks are due to the substitution of calcium to barium. Fig. 2.3 shows that O *K* edge absorption spectra of XANES for $Y_{0.7}Ca_{0.3}Ba_2Cu_3O_{6.9}$ and $YBa_2Cu_3O_{6.9}$ thin films [108]. Zhang-Rice (ZR) band is conduction band, and the unoccupied states of orbital of the ZR band is related to the O *K* edge absorption spectra. The electric field of incident x-ray is perpendicular to c-axis. The intensity of the absorption peak in energy 528.3 eV (ZR band) means the hole number in the CuO_2 plane of YBCO cuprate superconductors. It was evident that the hole concentration was increased for $Y_{0.7}Ca_{0.3}Ba_2Cu_3O_{6.9}$ thin film than $YBa_2Cu_3O_{6.9}$ thin film at the same oxygen content near optimum doping, and this method indeed allowed us to access the overdoped regime of YBCO cuprates.

2.1.2.1 X-ray Diffraction

X-ray diffraction (XRD) measurements are particularly suited for structure characterization since they give much information about the microscopic (crystal structure) and macroscopic structure (texture). In the heteroepitaxy, it is very difficult to attain the epitaxial growth of superconducting thin films with high crystalline perfection because of dissimilarity of the lattice constants existing between the growing layer and its substrate crystal. Therefore, a more detailed crystallographic characterization will be required in order to clarify the growth mechanism and to find the optimum of the growth conditions for obtaining the better crystalline quality [109] in the samples.

The crystalline structure of films was analyzed by X-ray diffraction technique with Cu-Kα radiation with the wavelength λ=1.5418 Å and a resolution of 0.01°. The XRD diffractometer with the RIGAKU RU200B rotating anode diffractometer

was adapted, and operating voltage of 40kV and the filament current of 30mA were used.

The typical θ-2θ X-Ray Diffraction pattern for YBCO and Ca-YBCO thin films are shown in Figs. 2.4(a) and 2.4(b). Apart from the LAO (100) substrate diffraction peaks, only (00ℓ) peaks of the thin films are observed in both cases, indicating the excellent c-axis oriented crystallinity of the films and epitaxial relationships with the substrate. The c-axis lattice constants for YBCO and Ca-YBCO films at optimum doping are 11.68 Å and 11.66 Å. And this is the evidence that the substitution of calcium to yttrium in Ca-YBCO thin film do not introduce any significant distortion in the YBCO lattice. By the way, the best double side samples exhibit no appreciable differences in the superconducting properties between films deposited on the two different sides.

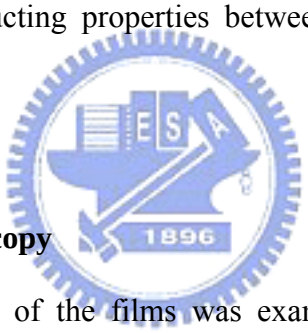

2.1.2.2 Atomic Force Microscopy

The surface morphology of the films was examined by use of atomic force microscopy (AFM) [34]. The tip of the AFM may be kept in direct contact with the surface in contact mode, or can be vibrated above the surface in non-contact mode. The contact mode is usually used at the repulsive-force about 10^{-10} ~ 10^{-6} Newton. The non-contact mode is used at the van der waals force for detection.

Figs. 2.5(a) and 2.5(b) depict the images of the surface morphologies of the YBCO films deposited on the LAO (100) substrate. The scanned area of the AFM image was 5×5 μm^2. It is evident that the films are grown by three-dimensional (3D) island formation. The average grain size of the film (see in Fig. 2.5(b)) is about 394±115 nm and the surface is rather smooth with mean roughness of 6.4±2.7 nm (see in Fig. 2.5(a)) comparing to microwave wavelength (~10 cm). Figs. 2.6(a) and 2.6(b)

also show the images of the surface morphologies of the Ca-YBCO films deposited on the LAO (100) substrate. The same surface properties were observed in contrast to YBCO thin film except the average grain size of the film (see in Fig. 2.6(b)) is about 153±24 nm and the surface mean roughness is 6.2±3.4 nm (see in Fig. 2.6(a)). Irregular grains with different sizes were observed in both films. Furthermore, because the roughness is much smaller than the penetration depth in our samples, then the surface of the microstrip resonators in our experiment can be viewed as near-ideal one.

2.1.3 Resistance (Resistivity) Measurement

The electrical resistance was measured by the standard four-probe technique in close-cycle refrigeration systems, which has capable of reaching operating temperatures as low as 20K. The contacts on films were made with thin copper wires by introducing silver dots and a constant current has (0.1 mA) been applied in the wire. The criterion of defining zero resistance was 1μV by the Keithly 181 Nanovoltmeter and Keithly 2001 Multimeter. The voltage was obtained by alternating direction of current flow and eliminating the thermal-electric effect. The data were recorded by a personal computer via an IEEE interface card. The resistivity cannot be obtained directly and needs to be extracted from the resistance measurement of thin films patterned into the microbridges.

The resistance measurements allow us to test the superconducting properties of the as-grown films. The as-deposited films were all c-axis oriented, with a typical thickness of 500 nm and T_c of 91 K for the YBCO thin film and T_c of 60 K for the Ca-YBCO thin film (see in Fig. 2.7) [110, 111], where T_c was determined from the zero resistance. From the temperature dependence of the resistance for the

$Y_{0.7}Ca_{0.3}Ba_2Cu_3O_{7-\delta}$ thin film ($\delta \approx 0.05$), the extrapolated value of the resistance is not equal to zero at T=0K, and the reason maybe is due to lattice antisite disorder or defects after doping calcium impurities.

2.2 Device Preparation

One of the first practical applications of HTSC is in the area of microwave passive devices [112]. For this purpose, the devices are typically constructed with various forms of coupled microstrip resonators. Among them, the parallel-plate resonators are very convenient and useful for investigating the fundamental physical parameters of the HTSC films.

In preparing microwave device, we use photolithography and wet etching methods to pattern the YBCO and Ca-YBCO thin films into micostip ring and line resonators or microbirdges for the resistivity measurements which have been employed in our work. The processes of fabricating microwave resonators were drawn schematically in Fig. 2.8 and the details are described as follows:

(1) The sample was cleaned ultrasonically for 12 minutes in acetone and 3 minutes in D. I. water and then it was dried with N_2 gas.

(2) Coating with the photoresist, AZ-5214E, on the thin films which was hold by a spinner. At begin stage, on the one hand, the spinning rate maintained with 1000 rpm in 10 seconds in order to uniformly spread the photoresist on the film surface. On the other hand, the higher speed (4000 rpm) was used to spin out the excess photoresist in 25 seconds in this stage. The thickness of the photoresist was about 1.7 μm on the YBCO or Ca-YBCO thin film.

(3) Pre-baking at 82 ^{o}C for 10 ~ 12 minutes in oven.

(4) Alignment and Exposure under the ultraviolet light for about 35 seconds with

proper masks.

(5) Development by a solution of composing of AZ-400K and D.I. water with the ratio 1:3 for 25~30 seconds, after rinse with D. I. water for 45~60 seconds, and check the sample to be development completed by the optical microscopy.

(6) Coating with the photoresist, AZ-5214E, at back of the thin films.

(7) Etching by a solution consisting of HCl and D. I. water with a ratio 1:40, after rinse with D. I. water for 30~60 seconds. To etch the YBCO or Ca-YBCO sample completely, we checked up the patterns by the optical microscopy.

(8) Rinsing the device with acetone to remove the photoresist on the sample that was cleaned ultrasonically 10 minutes in acetone and 2 minutes in D. I. water and dries it with N_2 gas.

(9) Using the acetone to remove the photoresist on the mask.

(10) One side of the YBCO or Ca-YBCO thin film was then patterned into a microstrip ring or line resonator, as depicted schematically in Figs. 2.9 and 2.10. The line width, the outer radius of the ring and the length of the line are 0.5 mm, 3.625 mm and 7.0 mm, respectively. The coupling gap between the microstrip feeding line and the ring resonator is about 0.4 mm.

2.3 Oxygen-Controlling

In order to varying the hole concentration in the YBCO or Ca-YBCO thin film, the oxygen-content controlling method is evitable to be the best choice for the measurements can be performed on the same film without introducing other phases in

YBCO structure. So, a reliable technique capable of precisely and reversibly controlling the oxygen content of YBCO and Ca-YBCO thin films is needed. We describe the technique and also report the experimental results of oxygen controlling in YBCO and Ca-YBCO thin films.

2.3.1 Oxygen-Controlling Procedure

The oxygen-content controlling system consists of high-temperature furnace, temperature controller, a quartz tube, some valves and three gauges used to monitor the pressure in the system, which has been described detail in Ref. [30]. The sample was placed in the quartz tube and the quartz tube was inserted into the furnace with a length of about 20 cm, and can be easily taken apart from the valve when keeping the pressure unchanged. The system was evacuated to a pressure of about 10^{-6} Torr using a turbomolecular pump prior. The desired oxygen contents of the YBCO and Ca-YBCO thin films were obtained by controlling the oxygen pressure and the corresponding temperature carefully which follows the pressure-temperature phase diagram established for YBCO system [113] (see in Fig. 2.11). In comparison with T_c vs oxygen content (δ) for thin-film samples of $YBa_2Cu_3O_{7-\delta}$ and polycrystalline $YBa_2Cu_3O_{7-\delta}$ [114] (see in Fig. 2.12) complementary, the oxygen contents of the YBCO thin films were determined. This oxygen-controlling process had been verified to be capable of obtaining designated oxygen contents of YBCO films in a controllable, reproducible and reversible way [30]. Basically, in the manipulation of oxygen-controlling process, on the one hand, the process to control the oxygen stoichiometry of YBCO thin films is the same as that used by Osquiguil et al. [115] except that wider pressure and temperature ranges were used in our experiment. As in Refs. [30] and [116], the sample was first heated to a start temperature, and then the

system was filled with oxygen pressure, while an adjustment in both pressure and temperature until it reached the equilibrium state of the designated oxygen content of the sample and was maintained at this state for approximately 30 min. After, both the oxygen pressure and temperature of the system were then decreased simultaneously along the specific pressure-temperature phase diagram of YBCO system to reach the final equilibrium state of the designated oxygen content of the sample. The system was maintained at the final equilibrium state for another 30 min and then quenched in ice water (0 ^{0}C). On the other hand, another more convenient but still controllable and reproducible oxygen-controlling method has been reported by Chung *et al.* [107]. Their method was that the sample was heated to a fixed temperature and the system was filled with a fixed oxygen pressure, which corresponds to the equilibrium state of the designated oxygen content of the sample at that temperature and pressure. The whole assembly was situated in an oxygen-annealing chamber, and the sample was quenched in ice water. The reproducible behavior for each designated oxygen-content can be reference to Chung's master thesis [107]. Moreover, Figs. 2.13(a) and 2.13(b) show that the θ-2θ X-Ray diffraction pattern for $YBa_2Cu_3O_{7-\delta}$ (δ=0.1 and 0.25) and $Y_{0.7}Ca_{0.3}Ba_2Cu_3O_{7-\delta}$ (δ=0.1 and 0.25) thin films by using this oxygen-controlling method [107]. It was evident that the YBCO (00*l*) and Ca-YBCO (00*l*) crystal structure maintains the same crystalline after during the oxygen-controlling annealing treatments although the intensity of the diffraction peaks was varied. Based on the above reason, we took the oxygen-content controlling method reported by Chung *et al.* to control the oxygen content in the same sample. The desired oxygen contents of the $Y_{0.7}Ca_{0.3}Ba_2Cu_3O_{7-\delta}$ thin film were obtained by putting the $YBa_2Cu_3O_{7-\delta}$ film and the $Y_{0.7}Ca_{0.3}Ba_2Cu_3O_{7-\delta}$ film together in the quartz tube and the whole assembly was situated in an oxygen annealing chamber for just varying the oxygen pressure and

keeping the temperature at 450 ℃ in 30min. Then the quartz tube was quenched into the ice water at 0 ℃. The experimental conditions are optimal for changing the oxygen contents of the $YBa_2Cu_3O_{7-\delta}$ thin films according to the pressure-temperature phase diagram and it is noted that all the measurements can be performed on a single film. By using this method, we can control the oxygen content of the $YBa_2Cu_3O_{7-\delta}$ film and $Y_{0.7}Ca_{0.3}Ba_2Cu_3O_{7-\delta}$ film in the same condition precisely and reversibly. The experimental parameters of oxygen-content controlling for $Y_{0.7}Ca_{0.3}Ba_2Cu_3O_{7-\delta}$ and $YBa_2Cu_3O_{7-\delta}$ thin films are listed in Table 2.1. There are three Ca-doping samples, Ca-Y040305A, Ca-Y050406A and Ca-Y050527A. Fig. 2.14 shows that the temperature dependence of resistance for the $YBa_2Cu_3O_{7-\delta}$ thin films with various oxygen contents at δ = 0.05, 0.12, 0.15, 0.24, 0.26 and 0.5, which corresponds to the same oxygen contents of the $Y_{0.7}Ca_{0.3}Ba_2Cu_3O_{7-\delta}$ (Ca-Y040305A) thin film, respectively. Fig. 2.15 shows that the temperature dependence of resistance for the $YBa_2Cu_3O_{7-\delta}$ thin films with various oxygen contents, from which the oxygen contents of the $Y_{0.7}Ca_{0.3}Ba_2Cu_3O_{7-\delta}$ (Ca-Y050406A and Ca-Y050527A) thin films can be determined. It should be noted that in Table 2.1, when the oxygen pressure is very low (0.01 Torr or below 5×10^{-6} Torr for sample Ca-Y050406A), the oxygen content can not be determined with the help of YBCO thin film but can be estimated from the T_c of $Y_{0.7}Ca_{0.3}Ba_2Cu_3O_{7-\delta}$ thin films [108]. We emphasize here that each set of results reported in this dissertation, either the temperature dependence of the resistivity or other physical properties, was obtained from a single film subject to repeated cycles of treatment. Consequently, possible complications that may arise from individual film microstructures are minimized and the changes in physical properties presented below should be due mainly to the effects associated with the

oxygen content of the film.

Table 2.1. The experimental parameters of oxygen-content controlling for $Y_{0.7}Ca_{0.3}Ba_2Cu_3O_{7-\delta}$ and $YBa_2Cu_3O_{7-\delta}$ thin films which have been placed together in the same experimental condition.

	Pressure (torr)	T (^{0}C)	Time (minute)	Ca-YBCO T_c(K)	YBCO T_c(K)	$Y_{0.7}Ca_{0.3}Ba_2Cu_3O_{7-\delta}$, 7-δ
Ca-Y040305A Ca-YBCO	770	450	30	60	91.0	6.95
	350	450	30	68.5	88.5	6.88
	50	450	30	78.5	86.1	6.85
	7.0	450	30	73.5	70.0	6.76
	4.0	450	30	68	67.8	6.74
	2.5	450	30	48.5	51.9	6.5
Ca-Y050406A Ca-YBCO	770	450	30	61	90.7	6.95
	300	450	30	74.5	87.8	6.87
	3.0	450	30	62	60.2	6.65
	2.5	450	30	52.5	47.0	6.5
	0.01	450	30	42.5	*	6.15
	$<5\times10^{-6}$	450	30	37.5	*	6.1
Ca-Y050527A Ca-YBCO	770	450	30	74.5	90	6.9
	2.5	450	30	53	56.2	6.6

2.3.2 The Effects of Oxygen Stoichiometry on the Transport Properties of YBCO and Ca-YBCO Thin Film

In 2000, Juang et al. [117] have reported the typical in-plane resistivity as a function of temperature $\rho_{ab}(T)$ for $YBa_2Cu_3O_{7-\delta}$ thin films with various oxygen contents (see in Fig. 2.16) by using the oxygen-content controlling method described above. They have given a detailed discussion on $\rho_{ab}(T)$ with respect to the oxygen content and the temperature. For example, the dimensional cross over from 3D to 2D

of the excess conductivity in the undedoped regime showed the prominent role played by the chain oxygen in interlayer coupling at 7-δ = 6.7. Fig. 2.17 shows the temperature dependence of in-plane resistivity $\rho_{ab}(T)$ for the $Y_{0.7}Ca_{0.3}Ba_2Cu_3O_{7-\delta}$ thin films whose oxygen content was intentionally manipulated at δ = 0.12, 0.15, 0.22, 0.24, 0.26 and 0.85, respectively [107, 108]. The $\rho_{ab}(T)$ curves demonstrate that the film was electrically uniform with narrow superconducting transition width near optimally doping (δ = 0.22). As is also evident from Fig. 2.17, when the film was near the optimally doping, not only the T_c reaches a highest value (~ 80 K), but also the normal state resistivity $\rho_{ab}(T)$ exhibits a well-behaved linear-T dependence. At T = 0K, the extrapolated value of the resistivity is not equal to zero for each oxygen content, and the reason maybe is due to lattice antisite disorder or defects after doping calcium impurities. The film shows increasing normal state resistivity as oxygen content decreasing. In particular, the change of the normal state resistivity $\rho_{ab}(T)$ behavior with the decreasing oxygen content in the underdoped regime was quite dramatic and has been examined by Juang et al. [117]. The departure from linearity in underdoped regime that occurs at some characteristic temperature, T^*, somewhat above the T_c, was one of the first indications of the existence of the, so called, 'pseudo-gap'. The 'pseudo-gap' concept is discussed in detail by Luo et al. [12]. From the resistivity measurements together with the above-mentioned evidences, the sample is henceforth of high quality and is suitable for revealing the intrinsic properties of the Ca-YBCO thin films [110, 111].

2.4 Calibration and Microwave Measurements

In this work, we measure the microwave properties of the Ca-YBCO and YBCO thin films with various oxygen contents using the microstrip ring and line resonators. The whole microwave measurement system contains the low-temperature measuring system and microwave measurement equipment. The low-temperature measuring system consists of: a turbomolecular pumping system which was used to evacuate the entire system to a base pressure of 1×10^{-6} Totr, a temperature-controller, a vacuum tube and a liquid helium Dewar. The microwave measurement equipment, HP 8510C Microwave Vector Network Analyzer, as shown in Fig. 2.18, permits accurate measurements to be made with the minimum of effort. It consists of: the signal sources (synthesizer to provide the RF stimulus with frequencies 40 MHz up to 20 GHz) [118], the test set which provides signal separation and the first frequency conversion stage, the IF/Detector and the Display/Processor. The test set provides the points at which the device-under-test (DUT) is connected, signal separation devices to measure the four S-parameters, and the first frequency conversion stage of the receiver. The device to be tested is connected between the test set Port 1 and Port 2. The test set separates the signal produced by the source into an incident signal sent to the DUT and a reference signal against which the transmitted and reflected signals are later compared. It also routes the transmitted and reflected signals from the DUT to the receiver (IF/Detector). The receiver together with the display/processor, processes the signals and using the integral microprocessors to perform accuracy enhancement, displays the results in a variety of formats. In the operational viewpoint, the vector network analyzer measures four S-parameters in linear responses of a device.

Before measuring the microwave device, a measurement calibration procedure must be done because calibration greatly reduces repeatable systematic errors from

our measurements. The measurement calibration procedure transfers the accuracy of one's calibration standards to the measurement of the device. Since the response of the standards is known to a high degree of accuracy, the system can measure one or more standards, then use the results of these measurements to provide data to algorithms which process the measured data for display. This process is called measurement calibration, accuracy enhancement, or error correction.

The detailed calibration steps at liquid nitrogen temperature (77 K) are described as follows:

1. Set up the frequency range to be measured

   Press START to input start frequency, and press STOP to input stop frequency.

2. Press CAL on display to select the type of calibration kit

   Press CAL 1, CALIBRATE and select FULL 2-PORT, then press REFLECT'N.

3. Calculate the reflection error coefficients (REFLECTIN)

   In order to calculate out the reflection error coefficients of S_{11} 1-PORT and S_{22} 1-PORT, we begin the calibration steps:

   I. Connect a standard Open Key at Port 1 of the DUT, and connect 50 ohms standard Load Key at Port 2 of the DUT. Then the DUT was placed into the vacuum tube. Next, we used the turbomolecular pump to have a background pressure below 1×10^{-6} Torr. The helium gas was then put into the vacuum tube about 400 Torr, and the vacuum tube was placed into the liquid helium Dewar. By connecting microwave signal cables with the transmission lines of the two ports, and also connecting the temperature controller with 8 pin signal heads, we turn on the power of the HP 8510C microwave network analyzer. It should be noted that during these processes we should put on the plastic gloves and use 8 lb-in handle to connect any connectors in avoid of any impedance mismatch. When the temperature is dropped down to liquid nitrogen

temperature (77 K), we press OPEN Key of S11and LOAD Key of S22 on display screen. After this, we turn off the power of the temperature controller and pull out the vacuum tube from the Dewar. Waiting for the temperature of the vacuum tube to rise to room temperature, we take out the Open Key and Load Key.

II. Connect the Port 1 of the DUT with standard Short Key, and connect the Port 2 of the DUT with Open Key. Using the method of step Ⅰ to pump out of the gas and connect the microwave signal cables with the transmission lines of the two ports, we then press SHORT Key of S11 and OPEN Key of S22 when the temperature is dropped down to liquid nitrogen temperature (77 K).

III. Connect the Port 1 of the DUT with Load Key, and connect the Port 2 of the DUT with Short Key. Using the same method of step Ⅰ to pump out of the gas and connect the microwave signal cables with the transmission lines of the two ports, we press LOAD Key of S11 and SHORT Key of S22 when the temperature is dropped down to liquid nitrogen temperature (77 K).

IV. After finishing the steps of I to III, press REFLECT'N DONE. The computer calculates out the reflection error coefficients promptly.

4. Calculate the transmission error coefficients (TRANSMISSON)

Press TRANSMISSION, and connect Thru Key with Port 1 and Port 2 of the DUT. Use the method of step Ⅰ to pump out of the gas and connect the microwave signal cables with the transmission lines of the two ports, we then press FWD TRANS. THRU to measure the frequency response of S21 when the temperature is dropped down to liquid nitrogen temperature (77 K). And we also press FWD. MATCH THRU to measure the load match of S21; press REV. TRANS. THRU to measure the reflection frequency response of S21; press REV. MATCH THRU to measure the reflection load match of S21. Finally, we press

TRANS. DONE. The computer calculates out the transmission error coefficients promptly.

5. Calculate the isolation error coefficients (ISOLATION)

Press ISOLATION, and connect Load Key with Port 1 and Port 2 of the DUT. Using the method of step Ⅰ to pump out of the gas and connect the microwave signal cables with the transmission lines of the two ports, then we press FWD. ISOL'N ISOL'N STD to measure the transmission noise of S21 when the temperature is dropped down to liquid nitrogen temperature (77 K). And we also press REV. ISOL'N ISOL'N STD to measure the reflection noise of S21. To press ISOLATION DONE, it stored the isolation error coefficients of S21 and S12.

6. Store the error coefficients of the above calculation

Press SAVE 2- PORT CAL to save the error coefficients of the above calculation. It needs only to press CORRECTION ON when measuring the test device.

7. Store and copy the calibration data to disc

If one wants to store the error coefficients of the calibration into a disc, one need press

DISC ➔ STORE ➔ CAL SET 1-8 ➔ CAL SET n ➔ CAL SET FILE n.

8. Recopy the storing data from a disc

If one wants to copy the error coefficients of the calibration on a disc to the network analyzer, one should press

DISC ➔ LOAD ➔ CAL SET 1-8 ➔ CAL SET n ➔ CAL SET FILE n.

9. Measure the test device

When measuring the microwave test device, the ground plane of the test device was stick to the base of the sample housing by using the silver glue. And the two ports of the test device were aimed to the two probes of the sample housing.

Locking the sample housing lightly with screws combined with springs, we put the sample housing into vacuum tube, and then used the method of step Ⅰ to pump out of the gas and connect the microwave signal cables with the transmission lines of the two ports. Then, we press CAL ➔ CORRECTION ON to measure the frequency response of the scattering parameter when the temperature is dropped down to liquid nitrogen temperature (77 K).

10. Store the measured data

The steps of storing scattering parameters are:

DISC ➔ STORE ➔ MORE ➔ DATA ➔ Input File Name ➔ FILE SAVE.

In a word, after performing the measurement calibration, the microstrip ring and line resonators made by YBCO and Ca-YBCO thin films was put into a gold-coated aluminum-designated sample housing with SMA connectors. The package was placed in a vacuum tube and immersed in liquid He. We used a Lake Shore 330 autotune temperature controller to control the temperature of the sample to better than 0.1 K. The temperature dependence of the resonance frequency f(T), frequency shifts $\Delta f(T)$ and the forward transmission coefficient S_{21} were measured by a HP8510C microwave vector network analyzer for different resonators.

The temperature dependence of the quality factor, Q(T), defined as $Q(T) = f / [(1-S_{21})\ \delta f]$, δf is the resonator bandwidth at –3 dB and S_{21} is the forward transmission coefficient, it is a measure of the sharpness of the response of the resonator to external excitation. Thus the surface impedance, $Z_s(T) = R_s(T) + jX_s(T)$, can be obtained in the microwave measurement within our system as follows. At first the real part of the impedance, the surface resistance R_s, determines the energy losses of an electromagnetic wave reflected from the sample and can be evaluated from the

relation of its Q-value, which can be expressed as $R_s = \Gamma/Q$, where Γ is the geometrical factor of the resonator [119, 120]. The imaginary part of the surface impedance, X_s, determines the non-dispersive energy store in the penetration depth of the superconductor. Once the values of R_s and X_s are obtained, the complex conductivity $\sigma = \sigma_1 - j\sigma_2$ can be yielded in terms of the two-fluid model assumptions. These physical properties measured by microwave resonators will be discussed in chapter 4. Here, we report the typical behavior of the temperature dependence of the resonant frequency $f(T)$ and scattering matrix S_{21} at T_c=90K for the YBCO film, as shown in Fig. 2.19. Note the abrupt increase for $f(T)$ at T_c caused by the screening supercurrents that reduce the kinetic inductance, according the LC circuits. In an homogeneous sample, the onset of such inductive transition coincides with the zero-resistance transition, at which macroscopic stable state for supercurrent is formed.

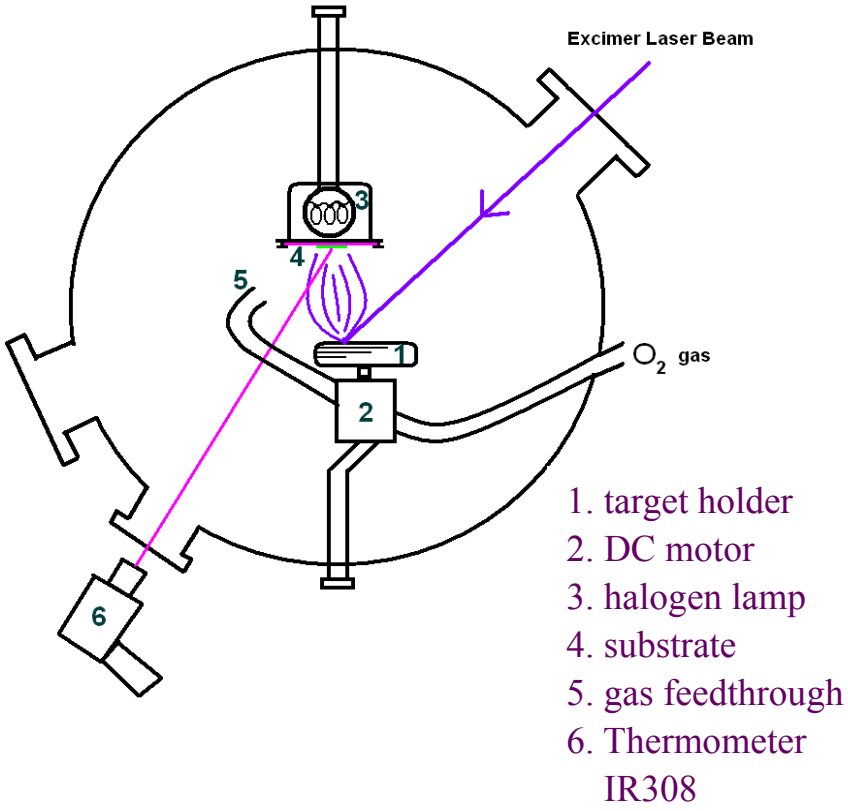

Fig. 2.1. Schematic diagram of the pulsed laser evaporation system for deposition of thin films.

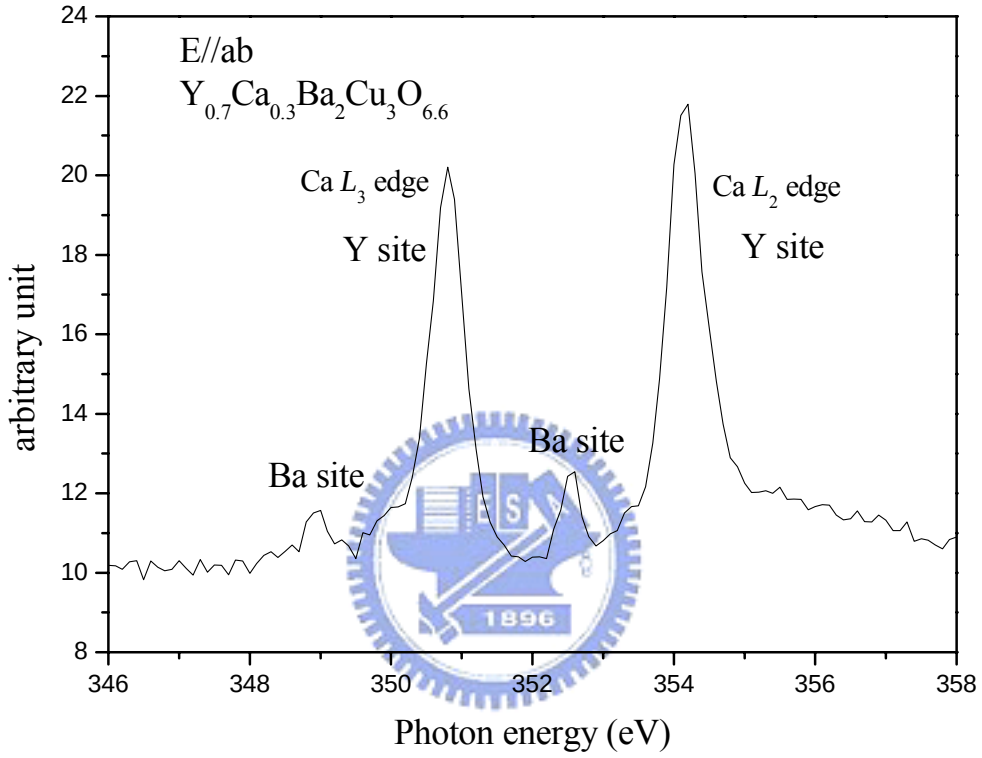

Fig. 2.2. Ca *L* edge absorption spectra for $Y_{0.7}Ca_{0.3}Ba_2Cu_3O_{7-\delta}$ thin film. The two highest absorption peaks are due to the substitution of calcium to yttrium. The lower absorption peaks are due to the substitution of calcium to barium [107].

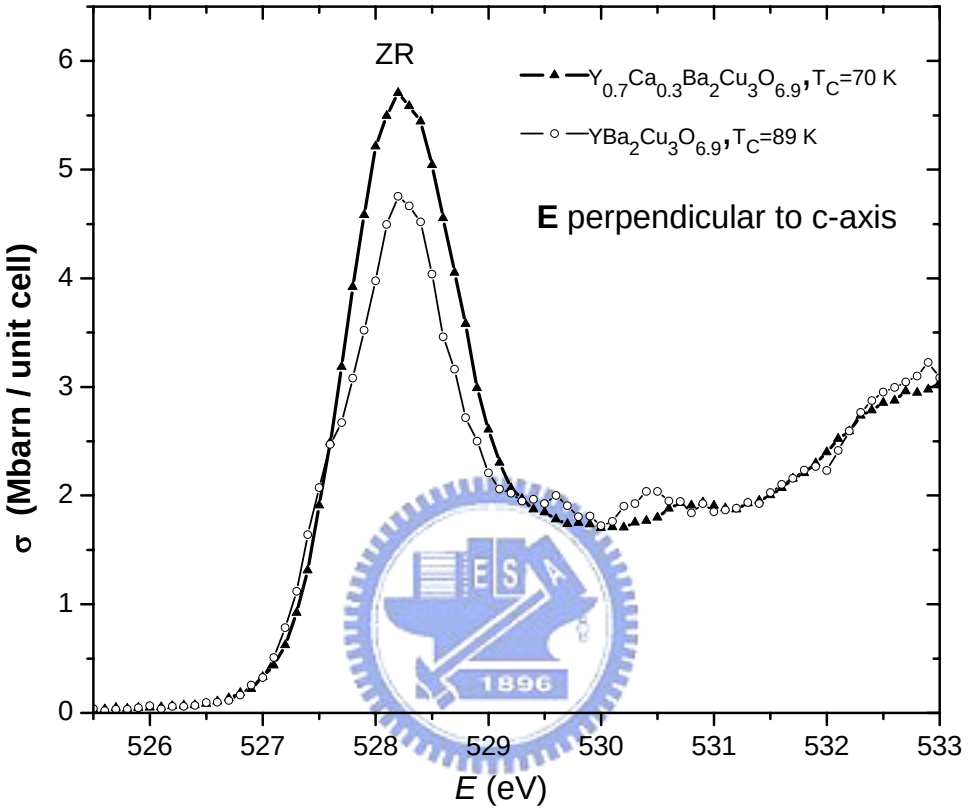

Fig. 2.3. O *K* edge absorption spectra of XANES for $Y_{0.7}Ca_{0.3}Ba_2Cu_3O_{6.9}$ and $YBa_2Cu_3O_{6.9}$ thin films. The electric field of incident x-ray is perpendicular to c-axis [108].

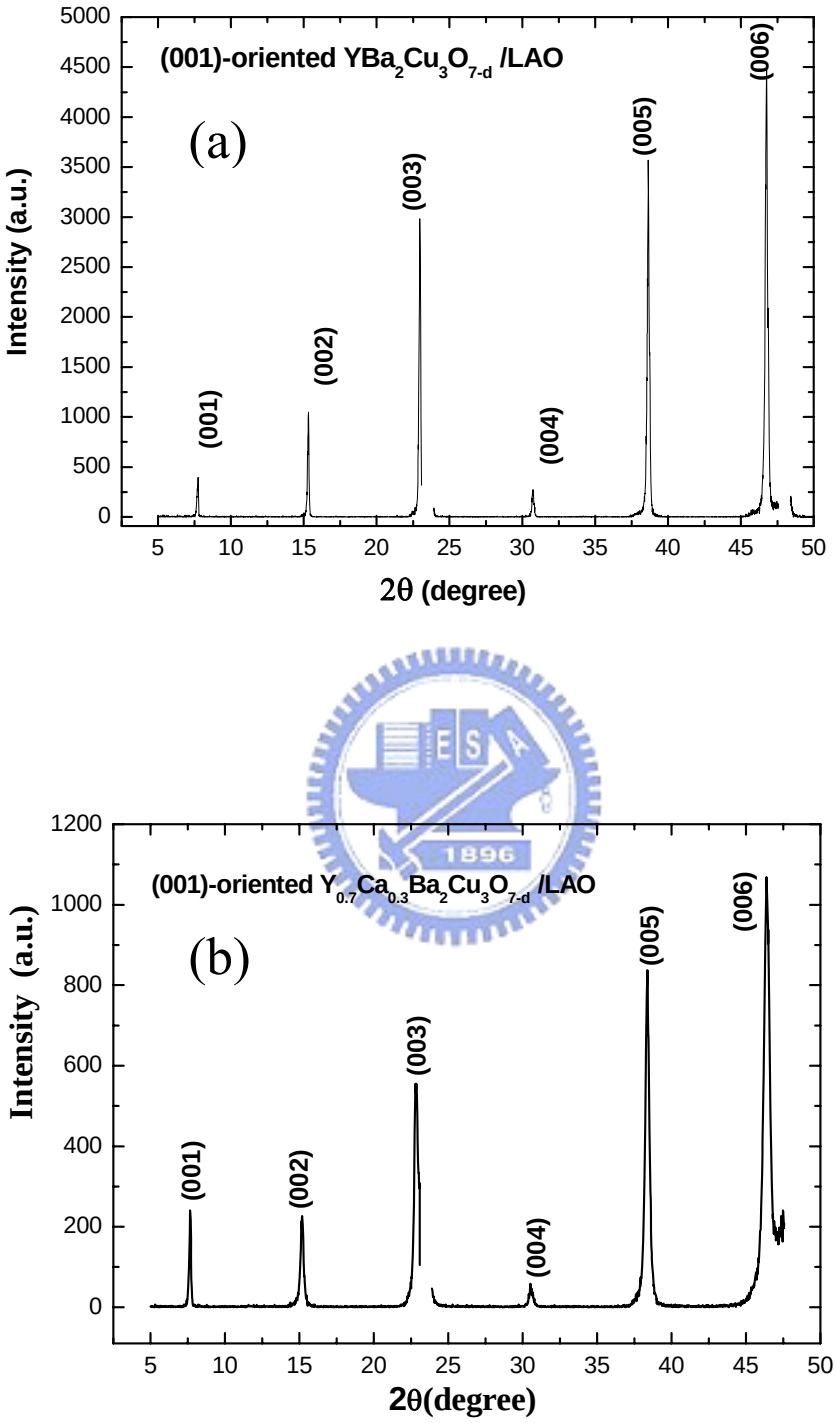

Fig. 2.4. The θ-2θ X-Ray diffraction pattern for (a) $YBa_2Cu_3O_{7-\delta}$ and (b) $Y_{0.7}Ca_{0.3}Ba_2Cu_3O_{7-\delta}$ films, respectively.

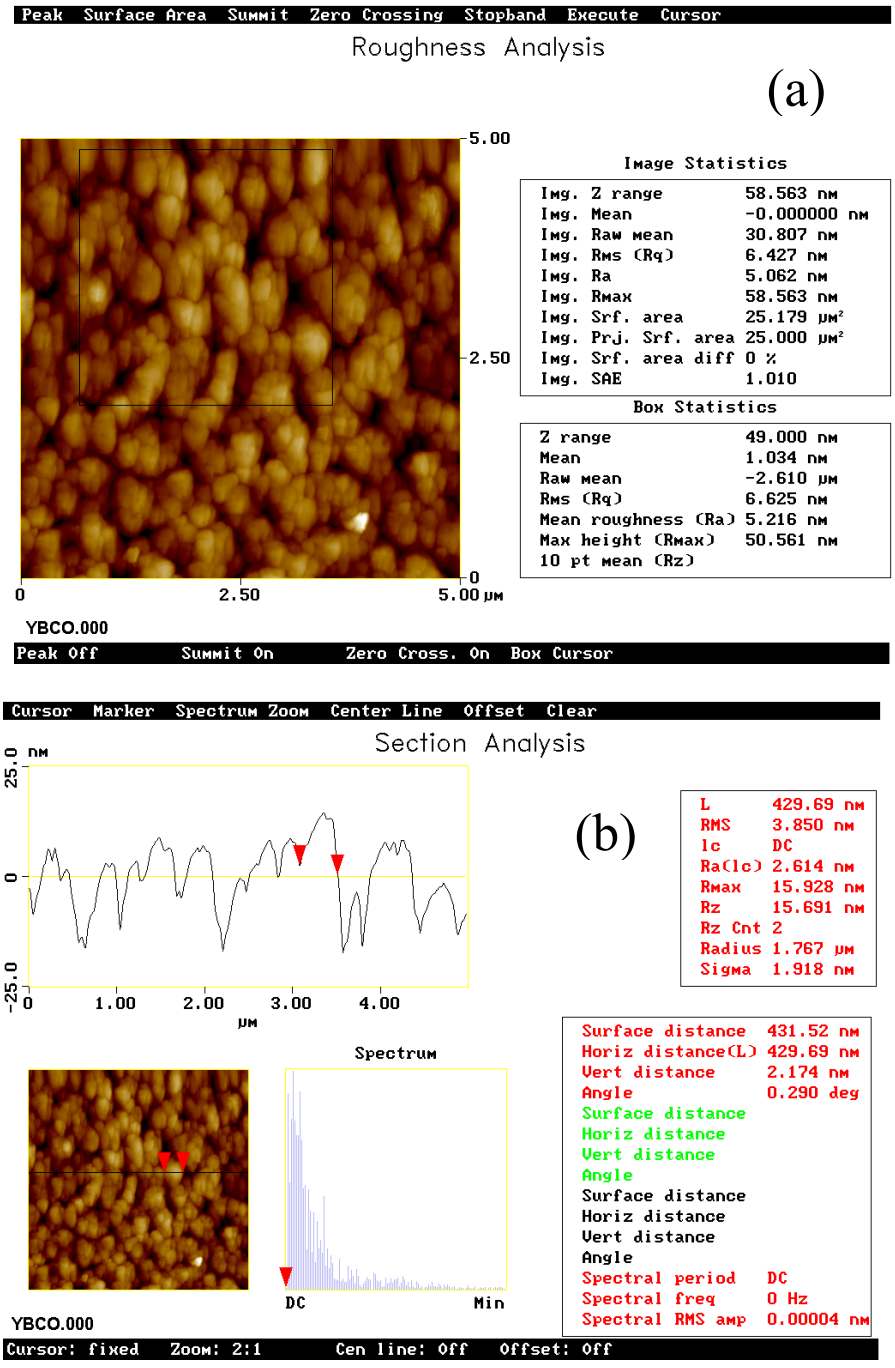

Fig. 2.5. The images of the surface morphologies of the YBCO thin film deposited on the LAO (100) substrate. (a). The surface roughness of the YBCO thin film was 6.4±2.7 nm. (b). The grain size of the YBCO thin film was 394±115 nm.

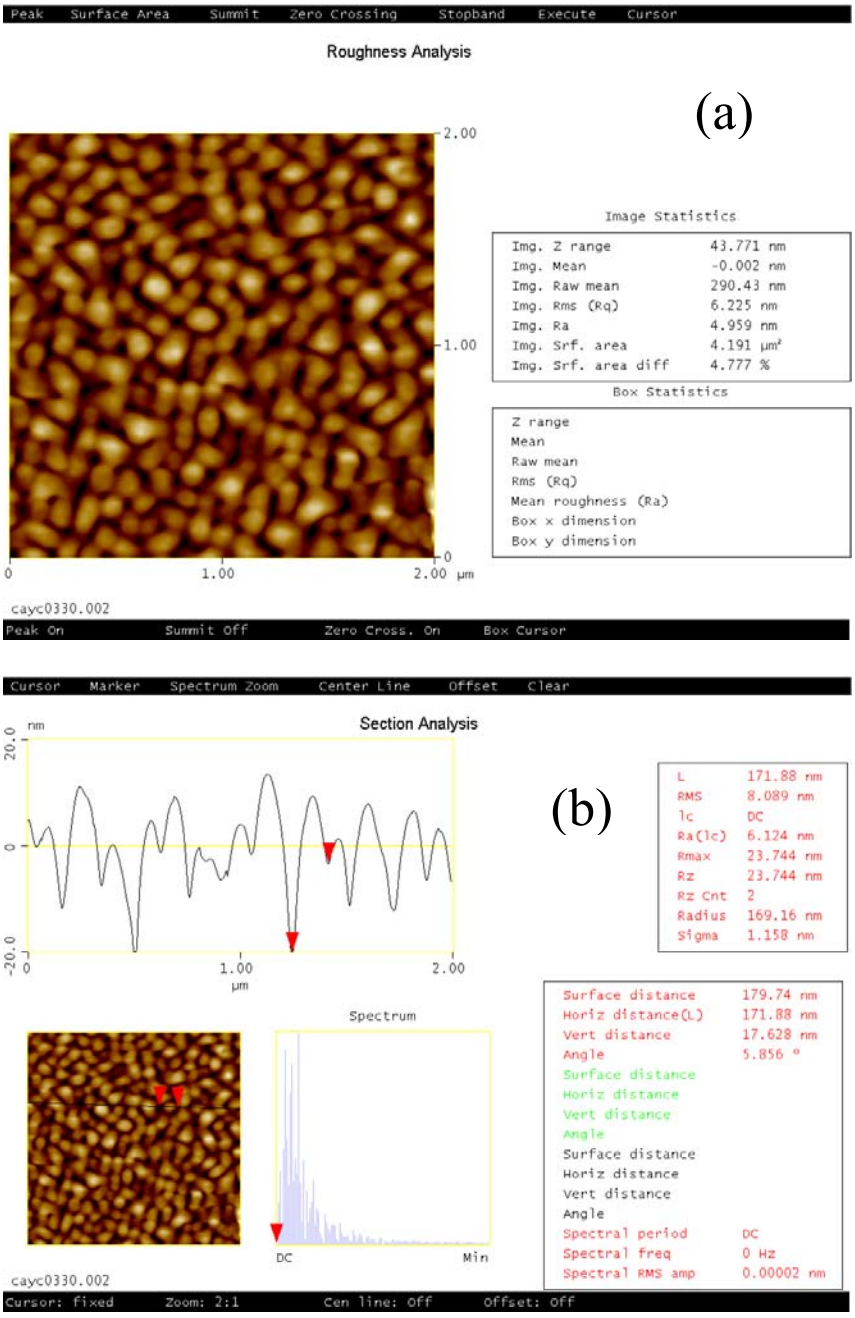

Fig. 2.6. The images of the surface morphologies of the Ca-YBCO thin film deposited on the LAO (100) substrate. (a). The surface roughness of the YBCO thin film was 6.2±3.4 nm. (b). The grain size of the Ca-YBCO thin film was 153±24 nm.

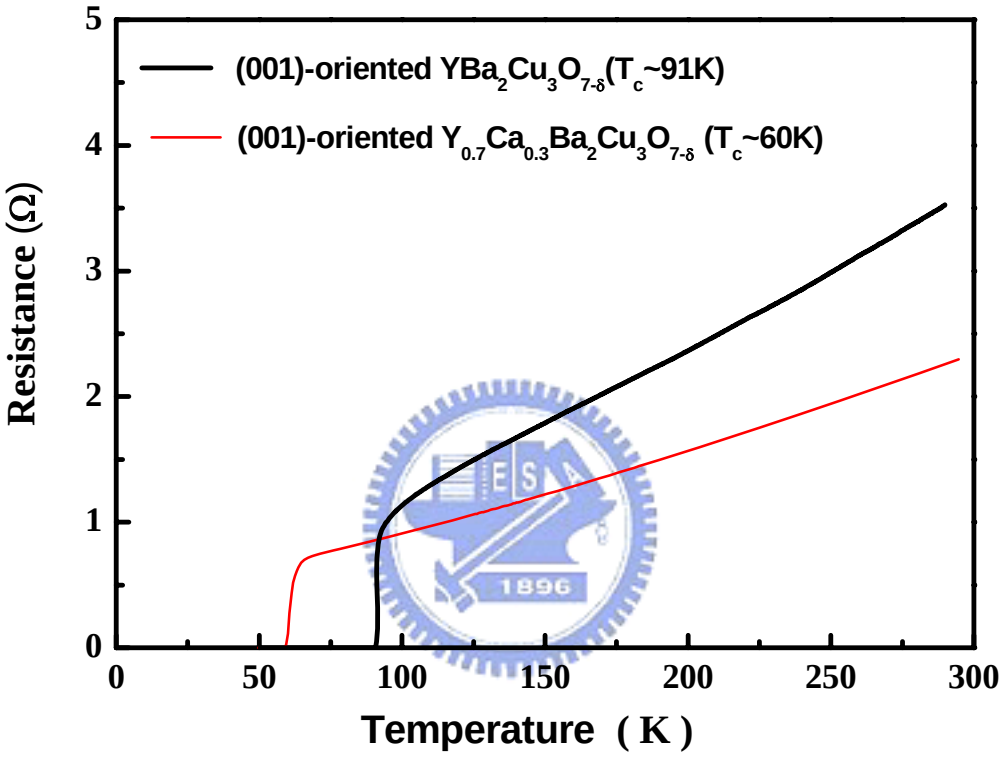

Fig. 2.7. The temperature dependence of resistance for the $YBa_2Cu_3O_{7-\delta}$ and $Y_{0.7}Ca_{0.3}Ba_2Cu_3O_{7-\delta}$ thin films ($\delta \approx 0.05$), which shows that the zero resistance critical temperature T_c~91K for $YBa_2Cu_3O_{7-\delta}$ film and T_c~60K for $Y_{0.7}Ca_{0.3}Ba_2Cu_3O_{7-\delta}$ film, respectively. At T=0K, the extrapolated value of the resistance of $Y_{0.7}Ca_{0.3}Ba_2Cu_3O_{7-\delta}$ film is not equal to zero, and the reason maybe is due to lattice antisite disorder or defects after doping calcium impurities.

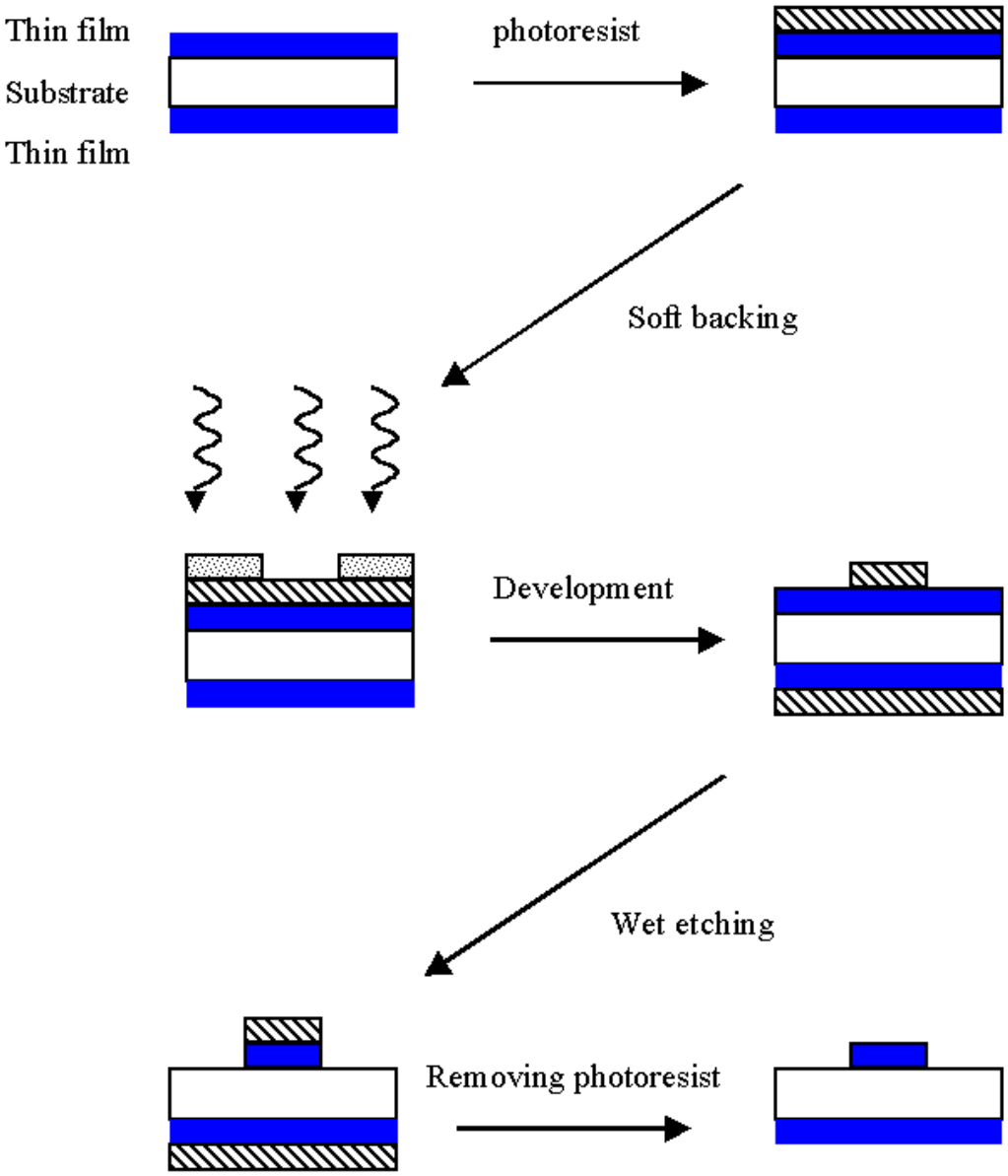

Fig. 2.8. The schematic diagram of the processes of patterning was described by the standard photolithography and wet etching method.

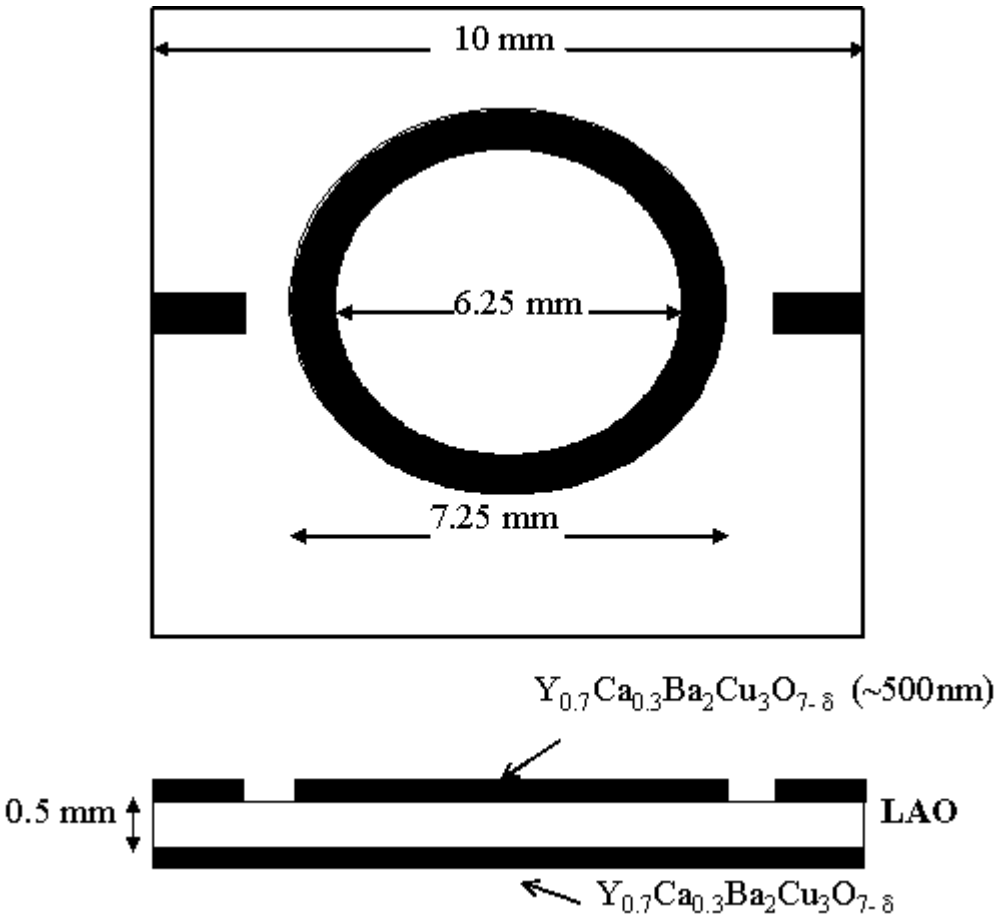

Fig. 2.9. The schematics of the ring-shaped microstrip resonator made of double-sided $Y_{0.7}Ca_{0.3}Ba_2Cu_3O_{7-\delta}$ thin films.

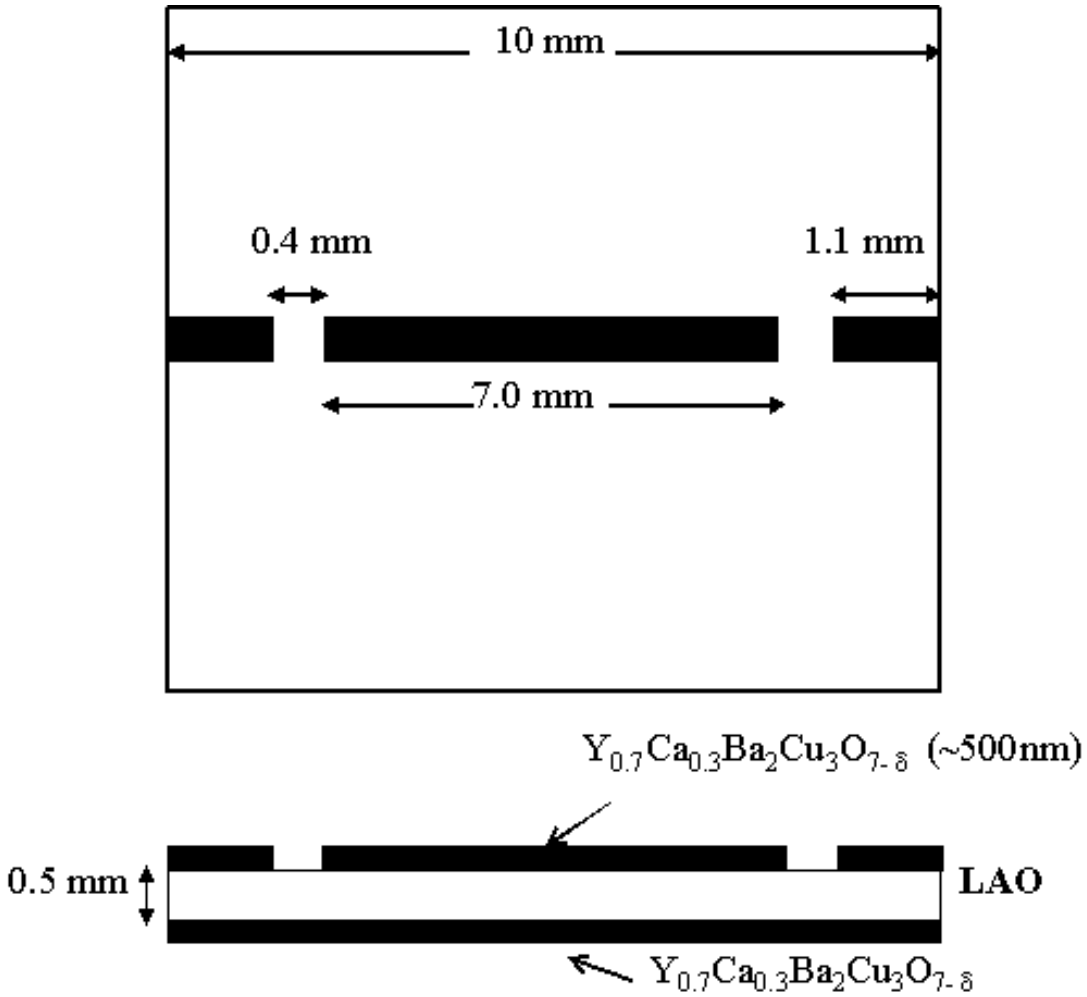

Fig. 2.10. The schematics of the microstrip line resonator made of double-sided $Y_{0.7}Ca_{0.3}Ba_2Cu_3O_{7-\delta}$ thin films.

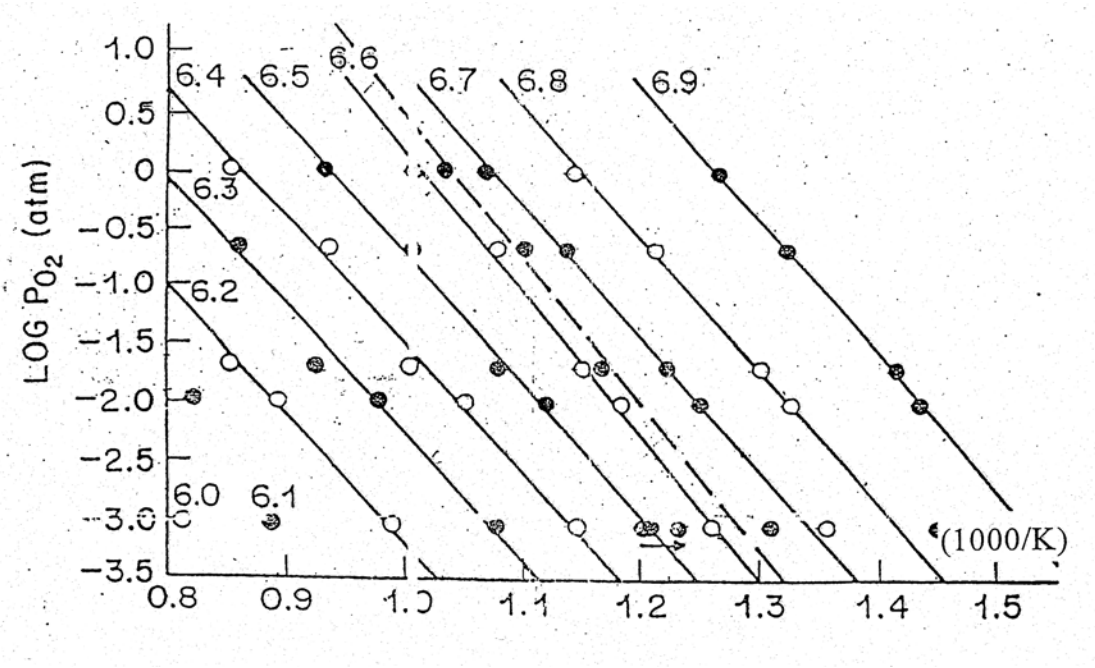

Fig. 2.11. The oxygen pressure-temperatrue phase diagram of YBCO bulk [113].

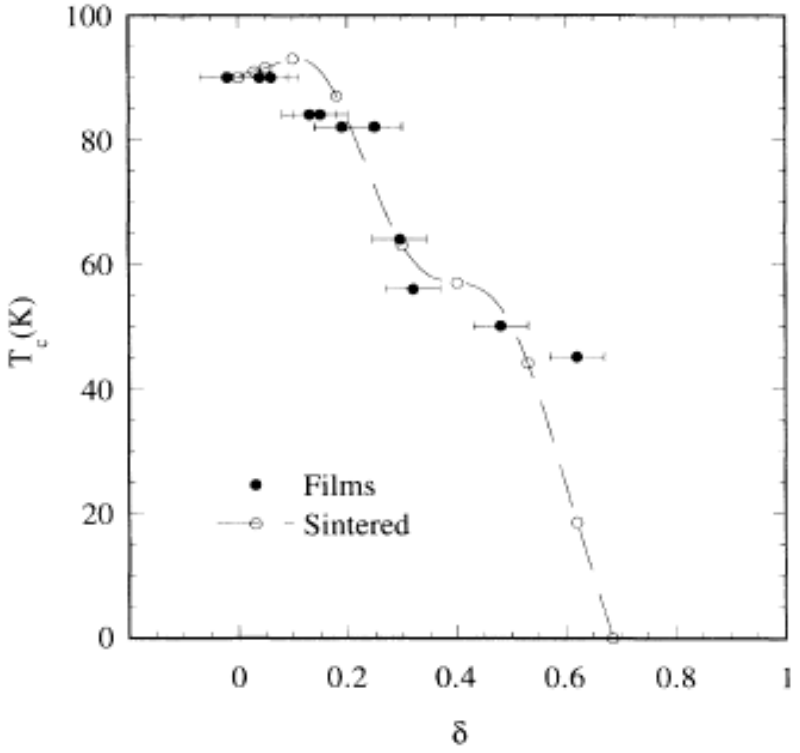

Fig. 2.12. Transition temperature (T_c) vs oxygen content (δ) for thin-film samples of $YBa_2Cu_3O_{7-\delta}$ and polycrystalline $YBa_2Cu_3O_{7-\delta}$. For the thin-film samples the values of δ were measured using electron probe microanalysis (EPMA), and for the sintered samples from weight loss [114].

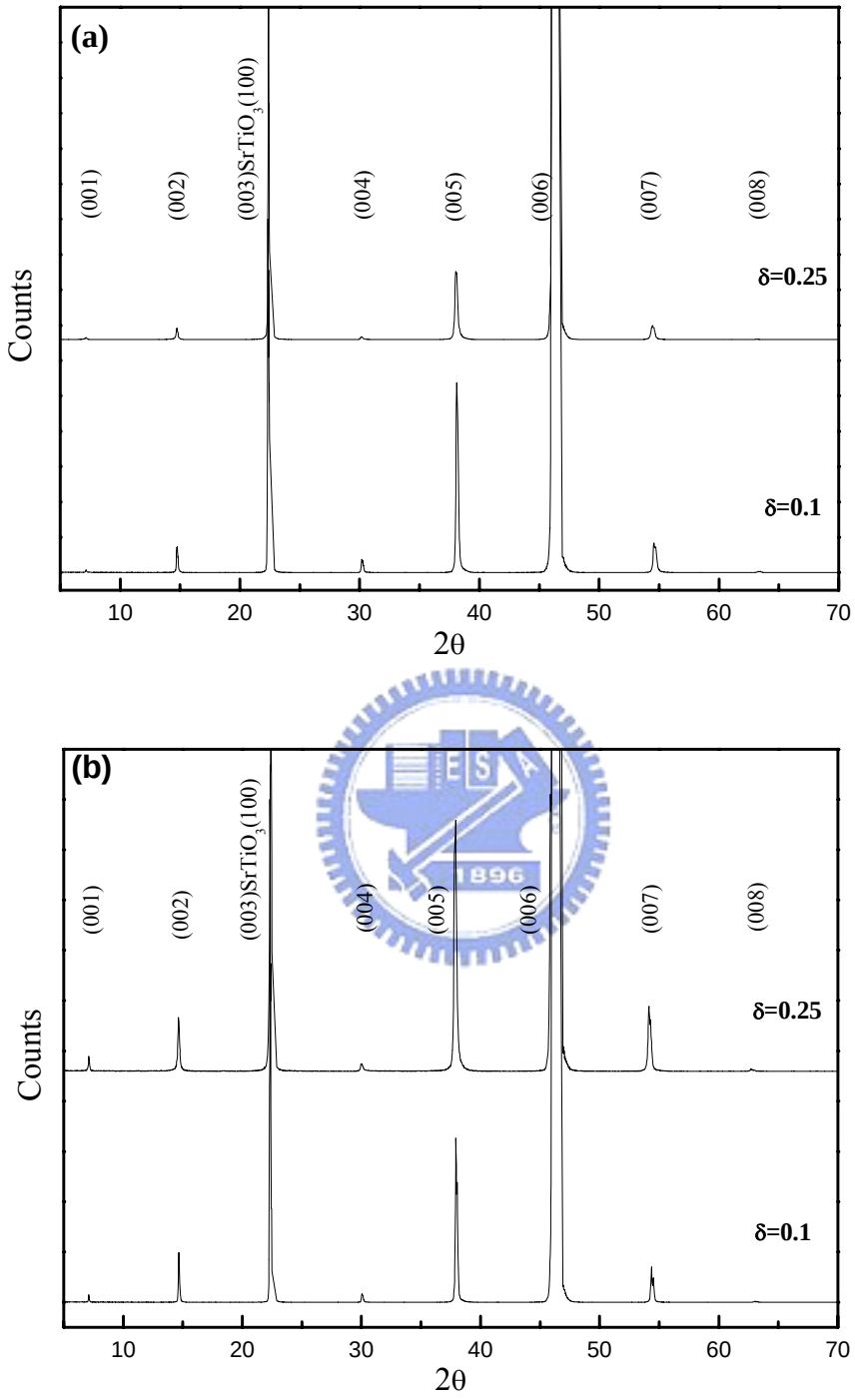

Fig. 2.13. The θ-2θ X-Ray diffraction pattern for (a) $YBa_2Cu_3O_{7-\delta}$ with δ =0.1 and 0.25 (b) $Y_{0.7}Ca_{0.3}Ba_2Cu_3O_{7-\delta}$ with δ =0.1 and 0.25, respectively [107].

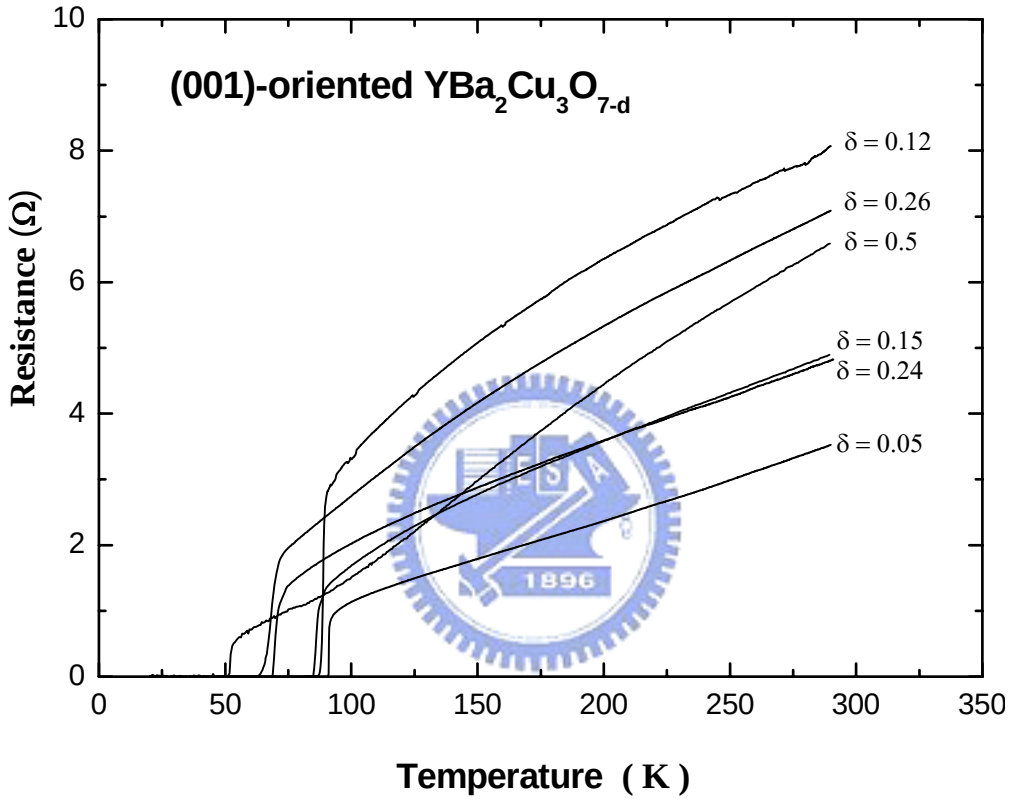

Fig. 2.14. The temperature dependence of resistance for the $YBa_2Cu_3O_{7-\delta}$ thin films with various oxygen contents at δ = 0.05, 0.12, 0.15, 0.24, 0.26 and 0.5,respectively.

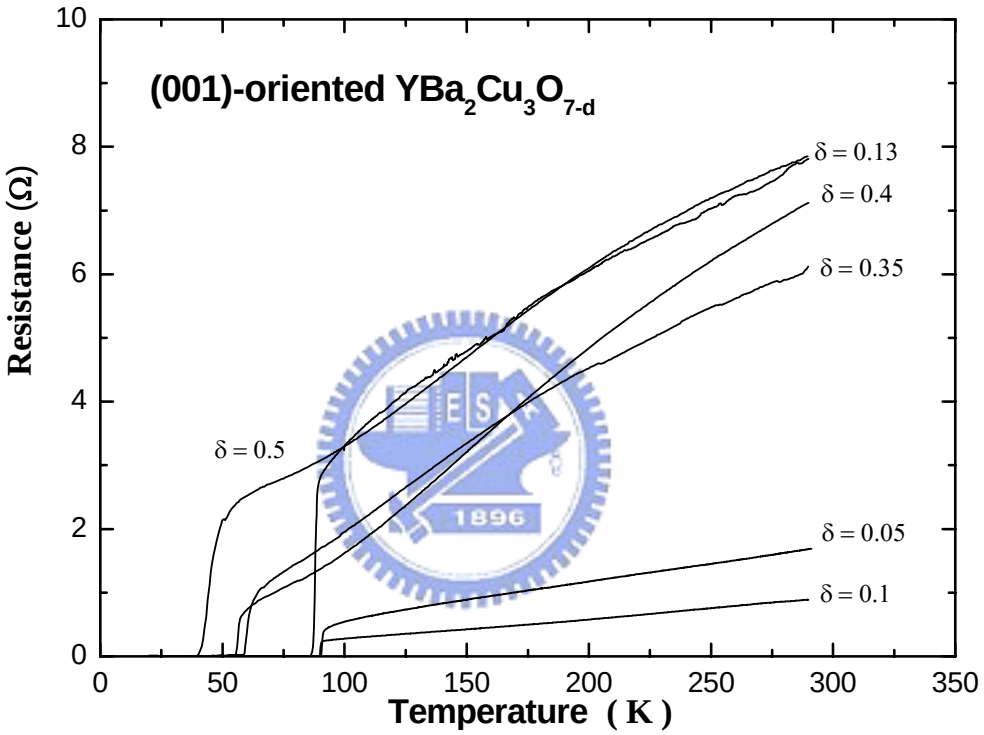

Fig. 2.15. The temperature dependence of resistance for the $YBa_2Cu_3O_{7-\delta}$ thin films with various oxygen contents. Note that the resistance are measured form various YBCO samples.

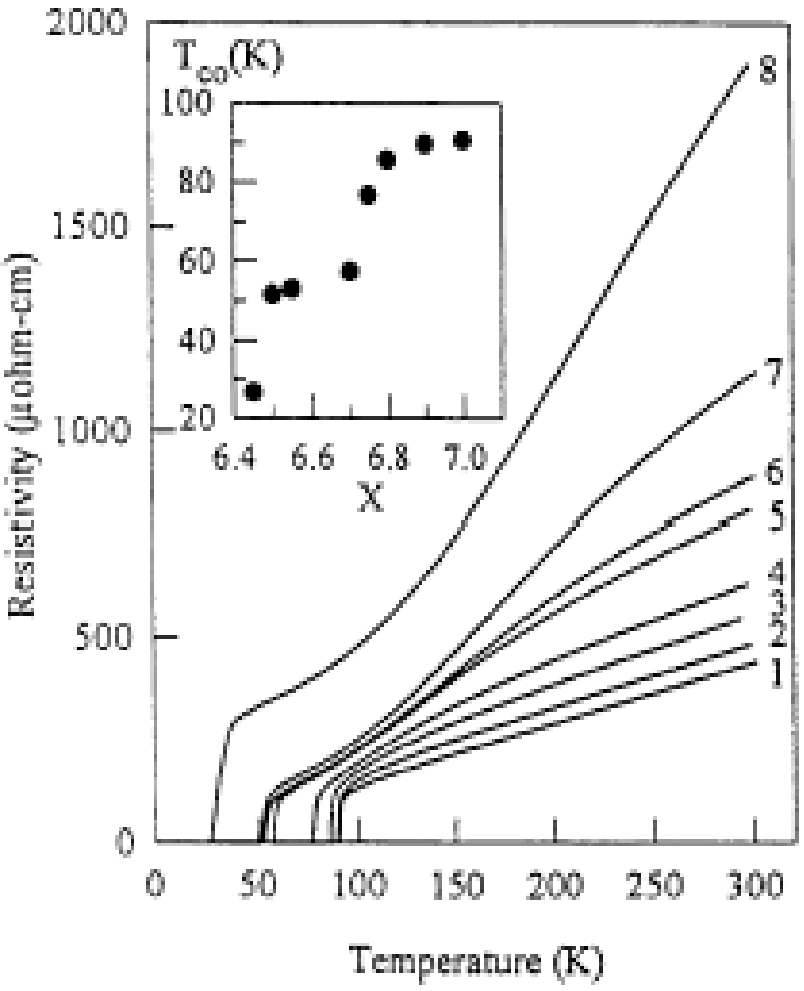

Fig. 2.16. $\rho_{ab}(T)$ for a YBCO film with various oxygen contents [117]. Curves 1 to 8 represent 7-δ (=x) = 7.0, 6.9, 6.8, 6.75, 6.7, 6.55, 6.5, and 6.45, respectively. The inset shows the T_{c0} as a function of x.

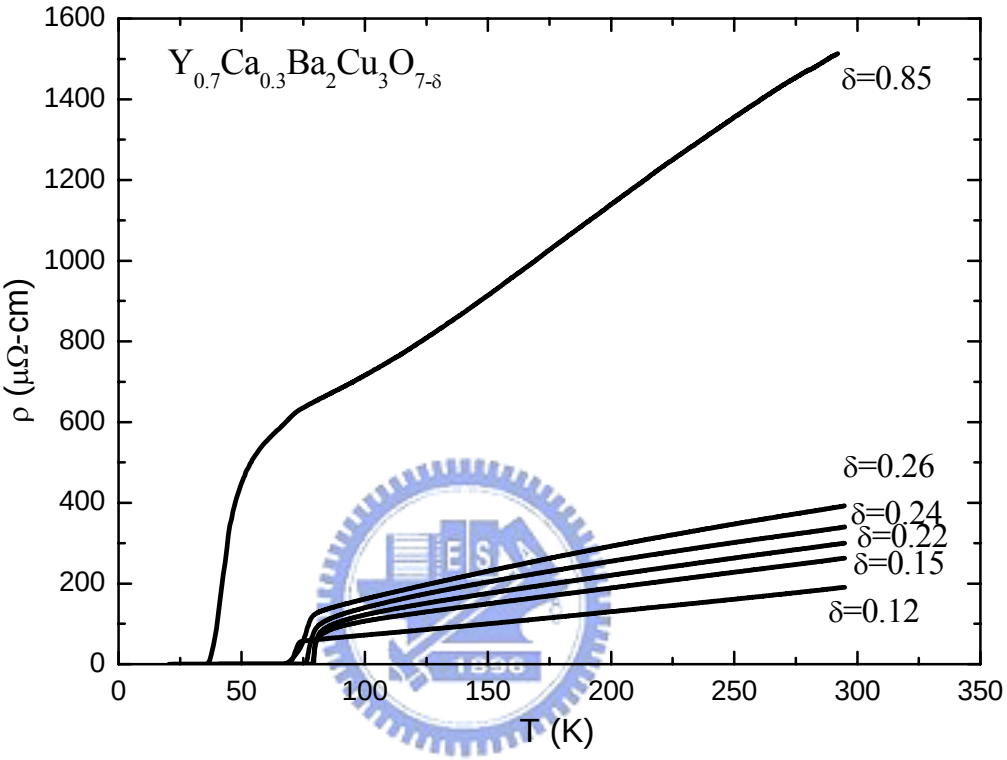

Fig. 2.17. The temperature dependence of d.c. resistivity for the $Y_{0.7}Ca_{0.3}Ba_2Cu_3O_{7-\delta}$ thin film with various oxygen contents.

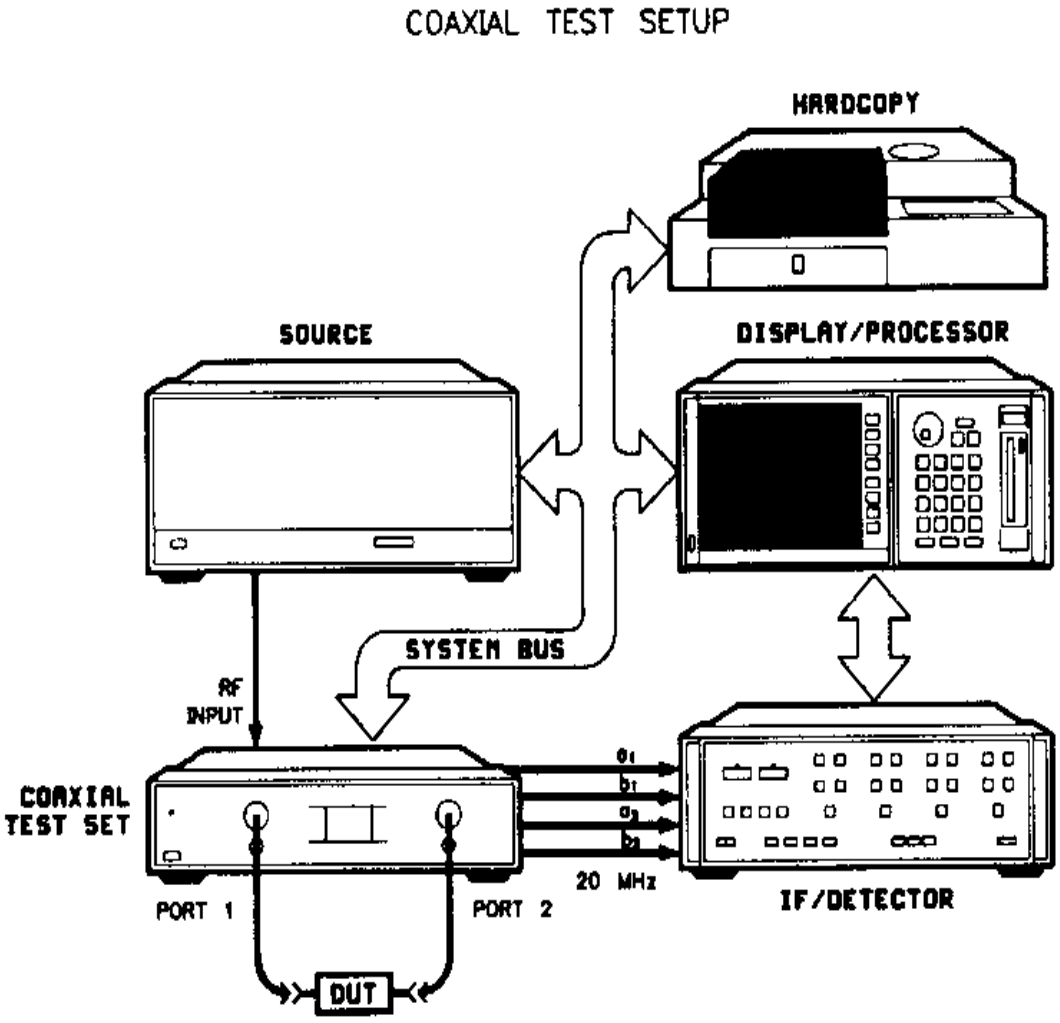

Fig. 2.18. The photography is a HP8510 C Network Analyzer to measure the scattering parameters of a one- or two-port microwave network from 40 MHz to 20 GHz.

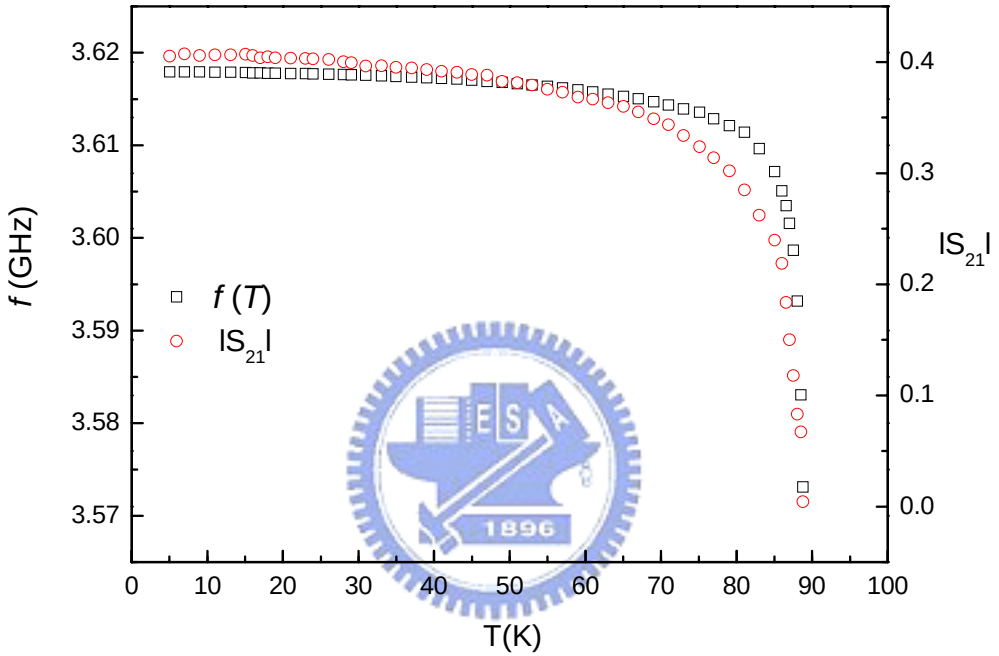

Fig. 2.19. The temperature dependence of the resonance frequency $f(T)$ and scattering matrix S_{21} at Tc=90K for the YBCO film. The abrupt change for $f(T)$ and S_{21} corresponds to the same critical temperature.